Mechanical Systems and Signal Processing 219 (2024) 111593

Contents lists available at ScienceDirect

Mechanical Systems and Signal Processing

journal homepage: www.elsevier.com/locate/ymssp

A multiresolution sparse signal representation approach for the decomposition of overlapping echoes in complex ultrasonic signals

Haotian Wang [a,b], Guangming Zhang [a,*], Hongwei Ma [b], Xuhui Zhang [b], Yuan Chen [b], David M. Harvey [a]

[a] General Engineering Research Institute, School of Engineering, Faculty of Engineering and Technology, Liverpool John Moores University, Liverpool L3 3AF, United Kingdom
[b] School of Mechanical Engineering, Xi'an University of Science and Technology, Xi'an, Shaanxi 710054, China

ARTICLE INFO

Keywords:
Sparse signal representation
Multiresolution analysis
Support matching pursuit
Gabor Dictionary
Ultrasonic signals

ABSTRACT

Modern 3D microelectronic packages frequently exhibit a significant overlap of reflected ultrasonic echoes, often exceeding 50 % due to the diminishing thickness of internal structural layers. This overlap results in a marked degradation of ultrasonic image quality during C-scanning. To tackle this issue, a novel multiresolution sparse signal representation algorithm is proposed to achieve multiresolution decomposition of overlapping ultrasonic signals.

The algorithm begins with SMP algorithm using a standard Gabor dictionary for initial decomposition. In each subsequent iteration, the dictionary is refined by narrowing the dictionary parameter boundaries while dividing the signal into shorter segments. Through this iterative refinement, the decomposition achieves increased precision without necessitating the enlargement of the dictionary size.

Our approach not only ensures a more precise decomposition but also enhances the alignment of dictionary atoms with ultrasonic echoes, especially in instances of echo overlap. The efficacy of this algorithm in accurately separating and estimating ultrasonic echoes has been validated through both simulated and experimental ultrasonic signals. This study strengthens Sparse Signal Representation (SSR) in ultrasonic Non-Destructive Evaluation (NDE) by addressing the challenge of unstable decomposition when the dictionary size surpasses a certain threshold, thereby enhancing the reliability of SSR in the failure analysis of 3D microelectronic packaging.

1. Introduction

Acoustic Microscopy Imaging (AMI) technology has been extensively employed in the reliability analysis of electronic packaging. Ultrasonic C-scan imaging generates interface images of testing materials at specific depths. To obtain a C-scan image, a pre-set time gate is applied to a series of A-scan signals collected by mechanically scanning the ultrasonic transducer over the test sample. Each A-scan signal comprises ultrasonic echoes reflected from various interfaces within the material. The maximum amplitude of each gated A-scan is stored as a pixel in the C-scan image at the corresponding X-Y scan position. However, the trend toward miniaturization in high-density electronic packaging, highlighted by the rise of Chiplet-based architectures, underscores the critical industrial demand for enhanced inspection techniques. The integration of Chiplets into compact electronic systems necessitates precise evaluation of

* Corresponding author.
E-mail address: G.Zhang@ljmu.ac.uk (G. Zhang).

https://doi.org/10.1016/j.ymssp.2024.111593
Received 16 February 2024; Received in revised form 22 April 2024; Accepted 30 May 2024
Available online 10 June 2024

component integrity and interconnections to ensure system reliability. This trend necessitates ultrasonic inspection methods of greater resolution. when inspecting multilayer microelectronic packages, if an internal layer's thickness falls below half of the ultrasonic wavelength or pulse width, overlapping echoes can result, cause echo distortion. Such echo distortion hampers precise defect localization and adversely affects the integrity of ultrasonic C-scan imaging. Moreover, these echoes are crucial as they encode essential defect characteristics, including size and type, which are imperative for effective ultrasonic Non-Destructive Evaluation (NDE). With the increasing need for higher precision in the detection of minuscule defects, the resolution offered by conventional Acoustic Micro Imaging (AMI) technologies is nearing its inherent limits.

Numerous methods have emerged in recent years, aimed at the enhancement of detected echoes within multilayer structures. These methods encompass techniques such as auto-correlation [1], adaptive filtering [2], autoregressive analysis [3], frequency spectrum analysis [4], and wavelet transformation [5]. Simultaneously, certain digital signal processing techniques, including compressed sensing [6], dictionary learning [7,8], and model-based methods [9], employ sparse constraints to process unique signals. The primary objective of these technologies is to augment defect detection and characterization. In our previous research, to address the issue of insufficient resolution when detecting internal defects in microelectronic packaging using traditional Acoustic Microscopy Imaging (AMI) systems, a novel AMI technique based on Sparse Signal Representation (SSR) was proposed, and a corresponding MATLAB toolbox was developed [10]. This innovation aims to break through the inherent resolution limitations of AMI in the assessment of microelectronic packaging. The technique employs nonlinear signal processing methods, utilizes an overcomplete time–frequency dictionary for sparse signal representation to characterize ultrasonic signals more flexibly, and achieves efficient identification and separation of ultrasonic echoes in A-scans, thus generating high-quality C-scan images.

In the past decade, Sparse Signal Representation (SSR) algorithms have advanced considerably, largely due to their inherent benefits in facilitating compact representations of signals and accomplishing super-resolution reconstruction. The SSR algorithm significantly improves detection accuracy by precisely aligning signals with predefined elements, known as 'atoms', within a dictionary. This is particularly evident in the non-destructive evaluation (NDE) of ultrasonic waves for multilayered electronic packaging. The analysis of ultrasonic signals in multilayer electronic packaging reveals a distinct characteristic: a finite number of echoes. This observation suggests that the signals could be sparsely represented in an appropriately selected signal dictionary, which is a core hypothesis of the Sparse Signal Representation (SSR) methodology. By exploiting this inherent sparsity, sparse decomposition techniques offer comparatively more precise and robust processing outcomes than conventional methods, thus highlighting their considerable value for practical applications.

Precisely because of this, there has been a growing interest in utilizing Sparse Signal Representations (SSRs) for ultrasonic Non-Destructive Evaluation (NDE) [11–13] In recent years. Ultrasonic echoes manifest as transient signals in A-scan and display time–frequency localization characteristics. Typically, SSR employs an overcomplete Gabor dictionary to characterize the echoes present within the ultrasonic signal during ultrasonic NDE. This Gabor dictionary comprises a series of waveforms, referred to as atoms. The SSR problem can be generalized as the following optimization:

$$\min_{x} \|x\|_0 \textit{subject to } Ax = y \tag{1}$$

Here, $\|x\|_0$ is the norm-0 of x ($x \in R^M$). which counts the number of non-zeros in x, while y denotes the given signal. The overcomplete dictionary A is an $M \times N$ matrix with $M \ll N$, where M is the number of atoms and N is the length of y. As a result, the equation Ax = y is underdetermined and has numerous solutions. If A is known, the primary objective is to find a solution for Ax = y that minimizes the number of non-zero elements in x. However, discovering this solution is an NP-hard problem. Consequently, suboptimal solutions are sought, and three strategies including convex relaxation, non-convex local optimization and greed search are commonly used to develop SSR algorithms [14]. A comprehensive discussion on SSR and its application in ultrasonic NDE can be found in Zhang et al. [15]. Li et al. [16] developed a novel sparse decomposition method based on a highly matched atomic dictionary to address the issues of noise and echo interference in the detection of fouling in heat exchange tubes under complex environments. Mor et al. [17] proposed a sparse approximation approach to monitor the degradation of adhesive joints. Utilizes a compact Gabor atom dictionary and processes the ultrasonic signals before and after degradation through a two-stage approximation. Kirchhof et al. [18] proposed a method using Sparse Signal Recovery and Orthogonal Matching Pursuit (OMP) to improve ultrasonic detection and reconstruction of shadowed flaws in non-destructive testing.

Research on the application of existing SSR techniques to ultrasonic NDE has demonstrated SSR has a great potential in this field. However, the challenge lies in the fact that existing SSR algorithms often struggle to find the optimal solution. Moreover, SSR theory dictates that the algorithms only find the optimal solution when the overcomplete dictionary size, i.e., the number of atoms, is below a certain threshold due to cumulative coherence bound [19], beyond this threshold, sparse decomposition becomes unstable and unreliable. Finer discretization steps for the Gabor dictionary parameters are required to generate atoms that accurately match various ultrasonic echoes, which leads to a larger dictionary size. This contradiction between a smaller dictionary size and finer discretization steps severely limits the capabilities of existing SSR algorithms for ultrasonic echo separation and estimation.

In this paper, we propose a multiresolution analysis sparse signal representation algorithm for accurate ultrasonic echo separation and estimation in overlapping ultrasonic signals. The algorithm separates severely overlapped echoes by iteratively segmenting the ultrasonic signal into two segments in the time domain and decomposing the segment signals using Support Matching Pursuit (SMP) [20] over a refined discrete Gabor dictionary. During each iteration, a customized discrete Gabor dictionary is regenerated by compressing the upper and lower boundaries of the Gabor function parameters and refining their discrete steps. This process allows for significantly smaller discrete steps of the Gabor function parameters without increasing the Gabor dictionary size, thereby enhancing the matching degree between the atoms and ultrasonic echoes at each iteration. As the segment signals are decomposed at higher

resolution and accuracy, overlapped echoes that cannot be separated on coarser scales will be distinguished at finer scales. This gradually improves the accuracy of both echo separation and estimation.

The main novel contributions of this work are as follows:

1) A multiresolution analysis sparse signal representation approach

Existing sparse representation techniques for ultrasonic signals have limited resolution that hinders accurate decomposition of overlapping echoes. The proposed multiresolution analysis algorithm iteratively segments signals into shorter segments and refines dictionaries without increasing size, enabling higher resolution decomposition at each iteration. This improves echo separation and estimation for overlapping echoes.

2) Customized dictionary updating based on signal segments

Dictionaries are updated for each signal segment based on the estimated echo parameters, allowing compressed parameter spaces tailored to the segment. This improves matching between dictionary atoms and echoes without increasing dictionary size.

3) Gradually improving accuracy from coarse to fine scales

Decomposition at finer scales and with refined dictionaries separates echoes that could not be resolved at coarser scales. This gradually improves the accuracy of echo separation and estimation.

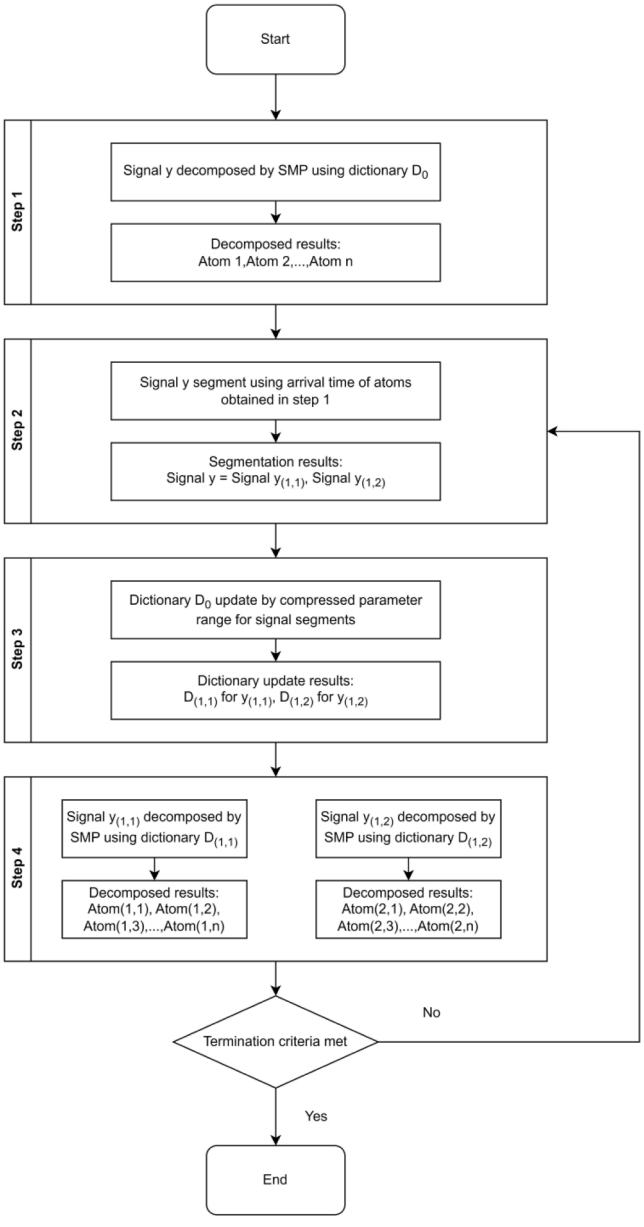

Fig. 1. Flowchart of the proposed algorithm.

In comparison to existing sparse representation methods for ultrasonic NDE that use fixed dictionaries, the key novelty and advantage of the proposed approach lies in the multiresolution analysis scheme with customized and refined dictionaries at each iteration. This enables higher resolution decomposition that more accurately matches dictionary atoms to ultrasonic echoes, especially for overlapped echoes.

The organization of this paper is as follows: Section 2 describes the proposed algorithm. Section 3 describes dictionary updating. Section 4 describes signal segmentation. Section 5 describes termination criteria for iteration. Section 6 presents the simulation results. In Section 7, the experimental results on real ultrasonic signals are given. Finally, Section 8 concludes this paper.

2. The proposed multiresolution analysis SSR algorithm

2.1. Discrete Gabor dictionary

The ultrasonic signal is a broadband pulse modulated at the transducer centre frequency and is commonly modelled by a Gabor function. A Gabor dictionary generated by discretising the four parameters (f, s, u, ω) of the Gabor function in equation (2) over the entire time–frequency plane is widely used in ultrasonic NDE:

$$g_\gamma(t) = \frac{1}{\sqrt{2\pi}s} e^{-\frac{(t-u)^2}{2s^2}} \cos(2\pi f(t-u) + \omega) \tag{2}$$

Where f represents the centre frequency of the atom, while s is the scale parameter that controls the atom's temporal width. The variable t denotes time, and u indicates the time position at which an echo reaches the receiver, reflecting the depth of the corresponding interface. Additionally, ω is the phase for an atom. This Gabor dictionary originally reported in Mallat and Zhang [21], and is generated by using the following discretization scheme: $\gamma = (f, s, u, \omega) = \left(ka^{-j}\Delta f, a^j, pa^j\Delta u, i\Delta\omega\right)$, $a = 2, \Delta u = \frac{1}{2}, \Delta f = \pi$, $0 < j < log_2 N$, $0 \le p < N2^{-j+1}, 0 \le k < 2^{j+1}$, where N represents the length of the signal. This Gabor dictionary is both succinct and complete [22]. However, due to the large discrete step size (more than 0.05 μs for time and 1 MHz for frequency) the accuracy of approximating ultrasonic echoes over this Gabor dictionary is often limited in ultrasonic NDE.

2.2. Advancing sparse signal decomposition with multiresolution analysis

Fig. 1 presents the flowchart of the proposed algorithm, with the operation steps summarized as follows:

Step 1: Initial sparse decomposition. The given ultrasonic signal y is decomposed using SMP over the standard overcomplete Gabor dictionary D_0 as described in Section 2.1.

Step 2: Signal segmentation. The ultrasonic signal y is divided into two segments $y_{(1,1)}$ and $y_{(1,2)}$ in the time domain by using the decomposition result in Step 1. The segmentation detail are described in Section 4.

The notation $y_{(1,1)}$ refers to the first signal segment obtained after the first signal segmentation.

The 1 on the left denotes the first iteration. The algorithm iteratively segments the signal into finer segments.

The 1 on the right denotes the first segment obtained in that iteration.

Step 3: Dictionary updating. A customized Gabor dictionary is generated for each segment by estimating the temporal widths, center frequencies, and spectral widths of the ultrasonic echoes based on the decomposed atoms from Step 1. The upper and lower boundaries of the Gabor function parameters are compressed, and a compressed parameter space is determined for each segment signal individually. Customized Gabor dictionaries, $D_{(1,1)}$ for $y_{(1,1)}$ and $D_{(1,2)}$ for $y_{(1,2)}$ are generated based on the compressed parameter spaces, as shown in Fig. 1. Details are described in Section 3. By compressing the Gabor dictionary parameter space, the discrete steps of the Gabor function parameters can be reduced without increasing the dictionary size, improving echo estimation accuracy due to better matching between dictionary atoms and ultrasonic echoes.

Step 4: Sparse decomposition of the segments using the customized dictionaries. Each segment obtained in Step 2 is decomposed using SMP and its corresponding dictionary obtained in Step 3.

Repeat the Step 2 and Step 3 until all the overlapped echoes are separated. The termination criteria are discussed in Section 5. For ease of expression, the segment i in iteration n is denoted as $y_{(n,i)}$, with its corresponding dictionary is denoted as $D_{(n,i)}$. At iteration n, there are 2^n segments. Iteration 0 corresponds to the initial decomposition described in Step 1. With each iteration, each segment siganl is further divided into two shorter segments, allowing the Gabor dictionary parameters in both time and frequency domains to be further compressed. As a result, the matching degree between atoms and ultrasonic echoes is refined. Since segment signals are decomposed at higher resolution and accuracy, overlapped echoes that cannot be separated on coarser scales are separated on finer scales.

3. Refinement and customization of Gabor dictionaries for enhanced echo decomposition

3.1. Parameter boundaries determination for dictionary customization

Assume m atoms denoted as $d_q (q = 1, 2, \cdots, m)$ are obtained after decomposing the given segment signal $y_{(n,i)}$ (i.e., the segment i at iteration n) in Step 2 of the proposed algorithm. The scale parameter, time position, centre frequency and phase of each atom can be represented as s_{dq}, u_{dq}, f_{dq} and ω_{dq} repectively. The lower boundary $sl_{(n,i)}$ for the parameter s can be estimated as $\min(s_{d1}, s_{d2}, \cdots, s_{dm})$,

and its upper boundary $su_{(n,i)}$ can be estimated as $\max(s_{d1}, s_{d2}, \cdots, s_{dm})$. Similarly, the lower and upper boundaries $ul_{(n,i)}$, $uu_{(n,i)}$, $fl_{(n,i)}$, $fu_{(n,i)}$, $\omega l_{(n,i)}$ and $\omega u_{(n,i)}$ can be estimated. The parameter boundaries for the customized dictionary $D_{(n,i)}$ are then determined as follows:

$$s \in \left[\frac{sl_{(n,i)}}{\alpha}, \alpha su_{(n,i)}\right], u \in \left[\frac{ul_{(n,i)}}{\alpha}, \alpha uu_{(n,i)}\right], f \in \left[\frac{fl_{(n,i)}}{\alpha}, \alpha fu_{(n,i)}\right], \omega \in \left[\frac{\omega l_{(n,i)}}{\alpha}, \alpha \omega u_{(n,i)}\right] \tag{3}$$

Where α is a relaxation coefficient to enlarge the boundaries. As the m atoms are obtained after sparse decomposition at a coarser scale, there may be mismatches between an atom and a true ultrasonic echo. By applying the relaxation factor, accurate ultrasonic echoes can be identified when the segment $y_{(n,i)}$ is decomposed over the customized dictionary $D_{(n,i)}$ at a finer scale in the next iteration n + 1.

3.2. Generation of customized Gabor dictionaries

The dictionary size of D_0, i.e., the number of atoms, denoted as L_{D_0} can be calculated by equation (4):

$$L_{D_0} = \sum_k^{2^{j+1}} \sum_p^{N2^{-j-1}} \sum_j^{log_2 N} \sum_i^{12} 1 \tag{4}$$

L_{D_0} is then used as the reference for the following dictionary customization. Employing the same discretization scheme and discretization steps as used in L_{D_0}, as described in Section 2.1, the dictionary size of $D_{(n,i)}$ for the segment signal $y_{(n,i)}$, can be calculated with the new boundaries estimated in equation (3), denoted as $L_{D_{(n,i)}}$. Since the parameter space is compressed, $L_{D_{(n,i)}}$ is smaller than L_{D_0} and the shrinking ratio $k_{(n,i)}$ can be calculated as:

$$k_{(n,i)} = \frac{L_{D_0}}{L_{D_{(n,i)}}} \tag{5}$$

This approach refines the discretization steps for the four parameters without increasing the dictionary size, addressing the trade-off between smaller dictionary size and finer discretization steps. Furthermore, there are multiple ways to generate a customized Gabor dictionary by creating different discretization schemes for these parameters. The development of an optimal discretization scheme will be explored in future research.

In ultrasonic NDT, the polarity of reflected echoes changes only when ultrasonic waves transmit from a material with higher density and speed of sound to one with lower density and speed of sound. In such cases, the reflected echoes alter their polarity at both interfaces. The polarity is influenced by the acoustic impedances and densities of the two materials, with acoustic impedances being determined by both the density and velocity of sound within the materials. As a result, the phase ω of ultrasonic echoes have very limited changes. Consequently, refining the parameter ω can be disregarded in this application.

In this paper, the customized dictionaries are generated using the discretization scheme outlined in Section 2.1 while refining the parameters s and f, the parameters u and ω are not refined. Although this is not the optimal scheme for updating the dictionaries, it can be employed to verify the proposed algorithm in Section 2.

Assume the number of sampling point for the scale parameter in the dictionary D_0 is ns_{D_0}. In dictionary D_0, $s = a^j, a = 2$, $1 \le j \le ns_{D_0}$, and $ns_{D_0} \le N$, with N being the upper boundary of scale parameter. To refine the discretization of scale parameter in $D_{(n,i)}$ to make $L_{D_{(n,i)}}$ is equal or close to the reference L_{D_0}, the variable a can be updated as follows:

$$a_{new} = \sqrt[ns_{D_{(n,i)}}]{su_{(n,i)}} = \sqrt[ns_{D_0}]{su_{(n,i)}} \tag{6}$$

The dictionary $D_{(n,i)}$ can be generated by employing the discretization scheme outlined in Section 2.1, taking into account the update boundaries estimated by equation (3) and the updated variable a_{new} calculated by equation (6). It is important to note that the parameter f is also refined, as it is related to the variable a_{new}.

4. Strategies for signal segmentation in sparse signal decomposition

In this section, we elaborate on the signal segmentation details used in Step 2 of the proposed SSR method. Assume there are m atoms in the given signal $y_{(n,i)}$ after sparse decomposition at iteration n. The process of segmenting $y_{(n,i)}$ into two segments can be summarized as follows:

1) Sort the m atoms in ascending order based on their arrival time u as $u = (u_1, u_2, \cdots, u_m)$.
2) Calculate the arrival time difference of two adjacent atoms, denoted as $du = (du_1, du_2, \cdots, du_{m-1})$.
3) Search for the largest du and assume it to be du_q. The given signal $y_{(n,i)}$ will be segmented at a time position between the two atoms of u_q and u_{q+1}.
4) Reconstruct two echoes from the atoms of u_q and u_{q+1} and their corresponding decomposition coefficients, denoted as echo(q) and echo (q + 1).
5) Assess if the two reconstructed echoes are overlapped. Different strategies are then taken to segment the given signal $y_{(n,i)}$. The details are described in the following.

For a reconstruct echo, its starting point A and ending point B, as depicted in Fig. 2, are defined as follow:

A is the point where the signal's amplitude begin to exceed a threshold from left to right, and B is the point where the amplitude of signal starts to surpass a threshold from right to left. Mathematically, A and B are calculated by equation (7):

$$A = \underset{t}{argmin}\{|y(t)| \geq \beta \max(|y(t)|)\} \tag{7}$$

$$B = \underset{t}{argmax}\{|y(t)| \geq \beta \max(|y(t)|)\}$$

Where β is a pre-set percentage, the threshold β will mainly affect the length of the segment signals. A lower β will lead to longer segment signals, which may potentially increase the iteration count n and slow down the convergence of the proposed algorithm. However, a higher β will lead to information loss. Therefore, in the case of noise, a relatively lower β is recommended.

We denote the starting point and ending point of echo(q) and echo(q + 1) are denoted as A_1, B_1, and A_2, B_2 respectively. If A_2 is smaller than B_1 as shown in Fig. 3 (a), the two echoes are overlapped. Otherwise, they are separated, as illustrated in Fig. 3 (b). If the two echoes are separated, the segmentation time position is set as the middle time position between B_1 and A_2, i.e., $u_s = (B_1 + A_2)/2$.

If the two echoes are overlapped, B_1 and A_2 are used as the segmentation points. Segment 1 comprises time position 0 to A_2 from the given signal $y_{(n,i)}$, while segment 2 spans time position B_1 to $N_{(n,i)}$, where $N_{(n,i)}$ denotes the length of $y_{(n,i)}$. Clearly, the two segments generated are overlapped. This approach ensures each echo is completely covered by a segment, and also prevents an echo from being truncate into different segments.

5. Termination criteria for iteration

At the iteration n, after SMP decomposition over the dictionary $D_{(n,i)}$, a given signal $y_{(n,i)}$ is represented as:

$$y_{(n,i)} = \sum_{k=0}^{m-1} < R^k y_{(n,i)}, g_{\gamma k} > g_{\gamma k} + R^m y_{(n,i)} \tag{8}$$

Assume m atoms are obtained for a given threshold ε of the residual signal $R^m y_{(n,i)}$. There exist two cases.

Case 1: m = 1. We update the dictionary $D_{(n,i)}$ to a finer dictionary $D_{(n+1,i)}$. $y_{(n,i)}$ is then further decomposed over $D_{(n+1,i)}$. There are two possibilities.

Case 1.1: The number of atoms obtained is still equal to 1 at the finer scale sparse decomposition, the iteration terminates and sparse decomposition for this segment signal ends.

Case 1.2: The number of atoms obtained is bigger than 1, the iteration continue until the Case 1.1 is met.

Case 2: m > 1. The iteration will continue and proceed to the finer scale. Until the case 1 is met.

6. Evaluating the MultiResolution SSR algorithm through simulation

6.1. Multiple echoes overlapping

The aim of this simulation is to evaluate the performance of the proposed SSR algorithm. A simulated ultrasonic signal y, comprising four echoes, is depicted in Fig. 4. Each echo is generated using the Gabor function, as described in Section 2.1, and their

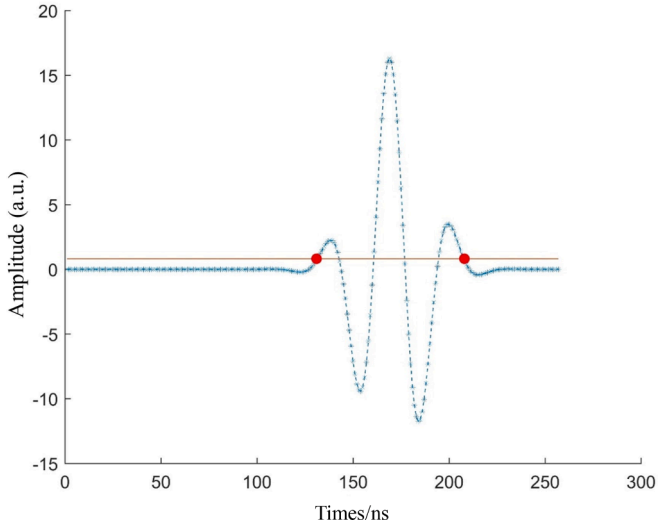

Fig. 2. The starting point and ending point of an echo with $\beta = 0.05$.

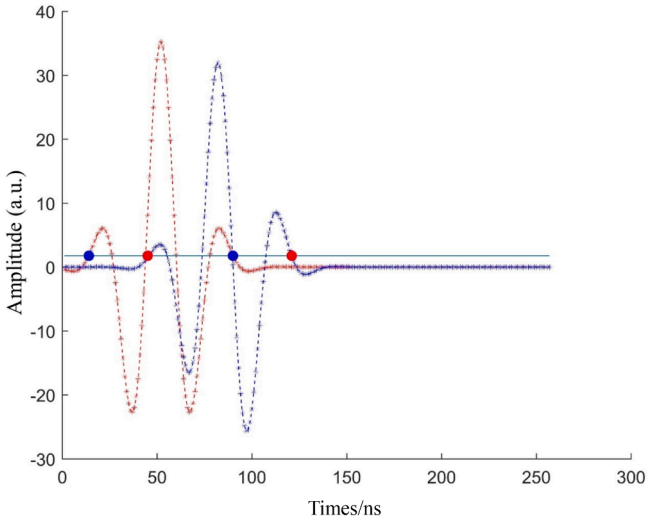

(a)

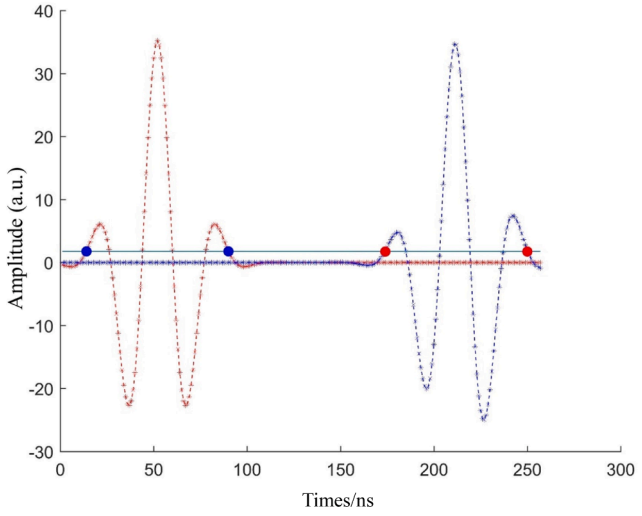

(b)

Fig. 3. (a) A simulated signal with two overlapped echoes; (b) A simulated signal with two non-overlapped echoes.

corresponding parameters are listed in Table 1.

The parameter values in Table 1 were selected to demonstrate and test the performance of the proposed multiresolution analysis algorithm through simulation.

The key aims in choosing the parameter values were twofold: 1) To simulate ultrasonic echoes with varying degrees of overlap; 2) To simulate echoes with different characteristics. This allows testing how the proposed algorithm separates and estimates overlapping echoes with variations in their parameters. The specific values for each parameter were selected as follows:

Frequency (f): All echoes were assigned the central frequency around 75 MHz to simulate echoes originating from a single ultrasonic transducer, Additionally, due to the attenuation of ultrasonic waves as they propagate within electronic packaging, the central frequencies of the four simulated signals progressively decrease.

Scale (s): Different scale values were chosen to simulate echoes with different durations, with larger scale corresponding to longer echoes. Corresponding to the central frequencies, the scales of the four simulated signals also decrease progressively.

Time position (u): Different u values were selected to simulate echoes arriving at different times, with a larger difference in u representing more separated echoes.

Amplitude: Larger amplitudes were chosen for Echoes 1 and 4 to show that the algorithm can handle echoes with different amplitudes.

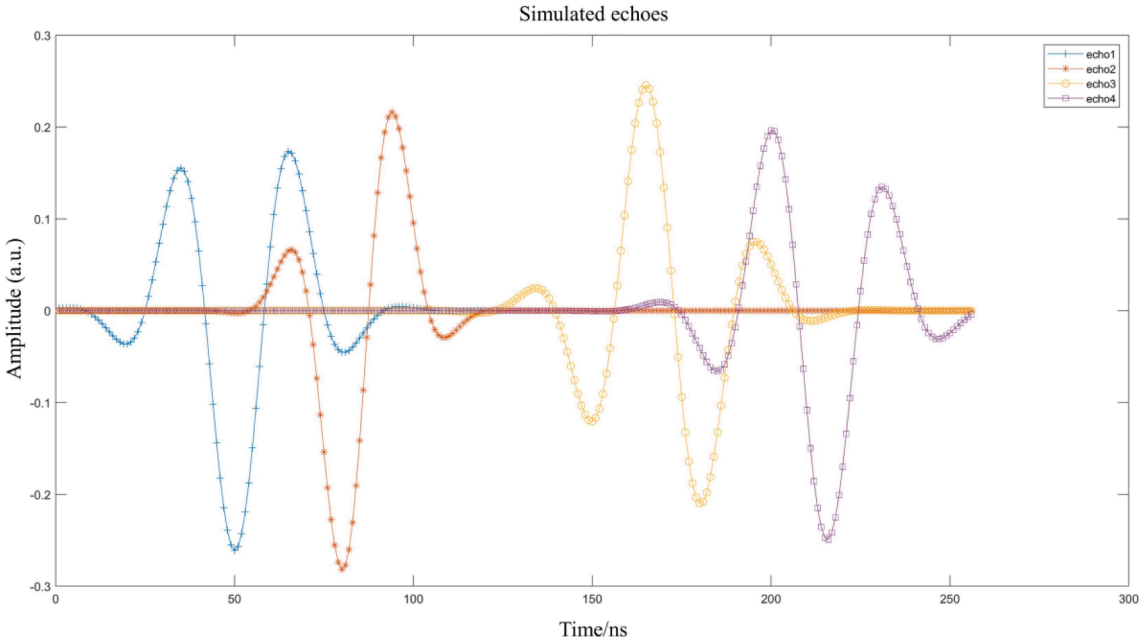

Fig. 4. The simulated ultrasonic signal, blue: echo1; brown: echo2; yellow: echo3; purple: echo4. (For interpretation of the references to colour in this figure legend, the reader is referred to the web version of this article.)

Table 1
The parameter used for the four simulated echoes.

Echo	1	2	3	4
$f(MHz)$	75	74	73	72
$s(us)$	0.017	0.017	0.0169	0.0168
$u(us)$	0.0510	0.0849	0.1699	0.2123
Amplitude	1.3	1.4	1.5	1.4

1) Initial sparse decomposition

The initial sparse decomposition is conducted using the SMP algorithm on the dictionary D_0. The threshold ε is set to 0.2, and four atoms are obtained after sparse decomposition on signal y. Fig. 5(a) displays the decomposition result in the phase plane [23], each atom is represented by a Heisenberg box. And the darkness of the box is represented by the decomposed coefficient of the atom, while Fig. 5(b) illustrates the reconstructed echoes. The parameters of the four atoms obtained are listed in Table 2.

In Fig. 5(b), the four subfigures are the matching comparisons between the four atoms obtained from the decomposition in Fig. 4(a) and the four echoes that compose the signal y. In these subfigures, the red curves represent the decomposed atoms, while the blue curves denote the initial echoes that make up signal y.

The atoms in Table 1 are sorted in ascending order based on their arrival time. Next, the arrival time difference between each adjacent atom is calculated, revealing that the largest arrival time difference is $du_2 = 64$, Consequently, atom No.2 and atom No.3 are chosen to segment the signal y into $y_{(1,1)}$ and $y_{(1,2)}$.

According to equation (7), the starting point and ending point of atom No.2 and atom No.3 are obtained : $A_1 = 0ns, B_1 = 153ns$, $A_2 = 94ns, B_2 = 256ns$. Since $A_2 < B_1$, atom No.2 and atom No.3 are considered as overlapped. Following the segmentation method outlined in Section 4, the signal y is divided into $y_{(1,1)}$ and $y_{(1,2)}$ by B_1 and A_2. The boundaries of each signal segment are: $y_{(1,1)} \in [0ns, 153ns], y_{(1,2)} \in [94ns, 256ns]$.

With the relaxation coefficient α set to 1.5, the compressed boundaries of scale parameter of the dictionary $D_{(1,1)}$ and $D_{(1,2)}$ can be obtained using equation (3) as: $s_{D_{(1,1)}} = [0.0437, 0.096]$, $s_{D_{(1,2)}} = [0.0437, 0.192]$.

The range of scale parameter in dictionary $D_{(1,1)}$ and $D_{(1,2)}$ is more compact than in dictionary D_0, results in fewer sampling point of scale parameter being reached during decomposition. To improve the system resolution, the discretization of s in $D_{(1,1)}$ and $D_{(1,2)}$ is refined to make $L_{D_{(1,1)}}$ and $L_{D_{(1,2)}}$ equal or close to the reference L_{D_0} by updating the variable a based on equation (6) as follows:

$$a_{new_{(1,1)}} = \sqrt[ns_{D_{(1,1)}}]{su_{(1,1)}} = \sqrt[ns_{D_0}]{su_{(1,1)}} = 1.7692284,$$

$$a_{new_{(1,2)}} = \sqrt[ns_{D_{(1,2)}}]{su_{(1,2)}} = \sqrt[ns_{D_0}]{su_{(1,2)}} = 1.9293573$$

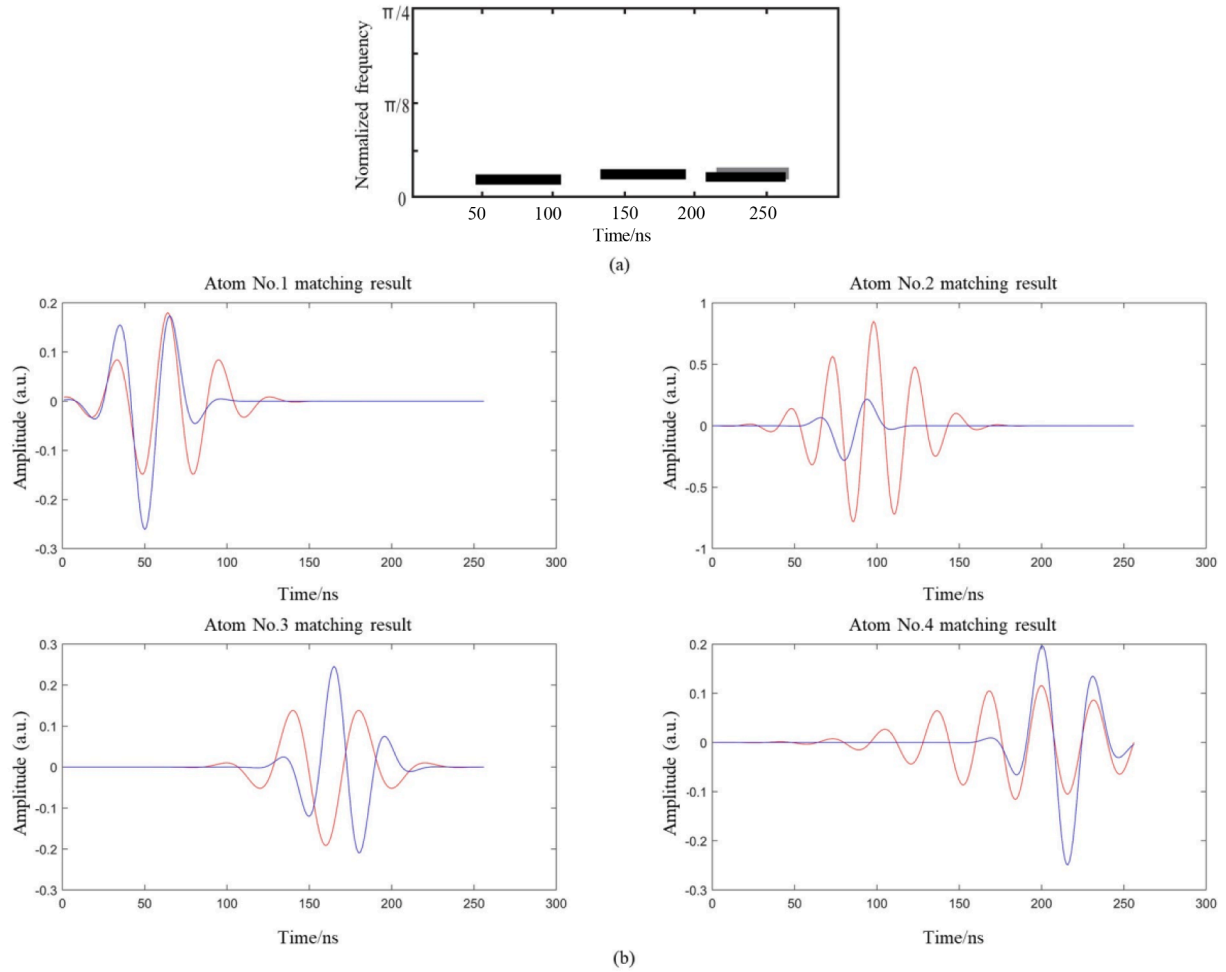

Fig. 5. The result of initial sparse decomposition (a) the decomposed result in the phase plane; (b) the reconstructed echoes matching with the four simulated echoes.

Table 2
The parameters of each atom obtained by the SMP algorithm over the dictionary D_0.

	$s(us)$	$u(us)$	$f(MHz)$
Atom1	0.064	0.064	78.5509
Atom2	0.064	0.096	75.0724
Atom3	0.064	0.160	76.4861
Atom4	0.128	0.192	71.1332

Compare to the dictionary D_0, the discretization step of scale parameter and frequency has been refined due to the step size a_{new} has become smaller. Simultaneously, the size of each dictionary can be calculated using equation (4).$L_{D_0} = 106496, L_{D_{(1,1)}} = 93184$, $L_{D_{(1,2)}} = 99265$.

2) Iteration 1

The signal segment $y_{(1,1)}$ and $y_{(1,2)}$ are decomposed using SMP through dictionary $D_{(1,1)}$ and $D_{(1,2)}$ respectively, by setting the residual threshold ε equal to the initial sparse decomposition. Fig. 6 displays both the decomposed results in the phase plane and the reconstructed echoes. As seen in Fig. 6, two atoms obtained for each signal segment.

In Fig. 6(b), the four subfigures are the matching comparisons between the four atoms obtained from the decomposition in Fig. 4(a) and the four echoes that compose the signal y. In these subfigures, the red curves represent the decomposed atoms, while the blue curves denote the initial echoes that make up signal y.

Since only two atoms obtained for each signal segment, signal $y_{(1,1)}$ is segmented into $y_{(2,1)}$ and $y_{(2,2)}$ based on the arrival time of its two atoms. Similarly, signal $y_{(1,2)}$ is segmented into $y_{(2,3)}$ and $y_{(2,4)}$. The starting point and ending point of the two atoms decomposed

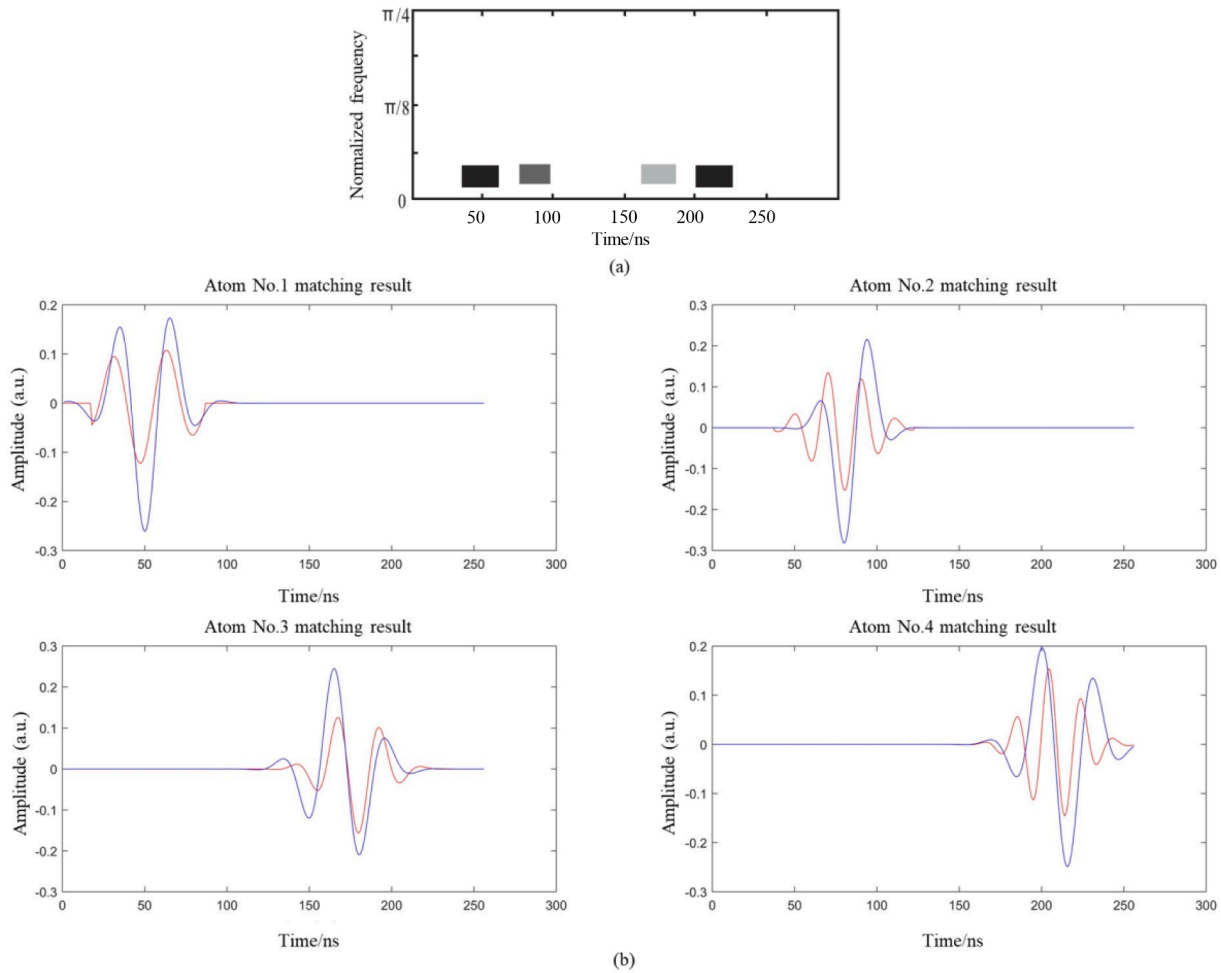

Fig. 6. The result of first iteration of the proposed algorithm (a) in phase plane; (b) matching with the simulated echoes.

from $y_{(1,1)}$ are determined by equation (7).

$$A_1 = 0ns, B_1 = 85ns, A_2 = 84ns, B_2 = 153ns$$

The starting point and ending point of the two atoms decomposed from $y_{(1,2)}$ can be obtained as well.

$$A_1 = 94ns, B_1 = 220ns, A_2 = 137ns, B_2 = 247ns$$

As $A_2 < B_1$ in both signal segment, the two atoms in each signal segment are considered overlapped. According to the segmentation method in Section 4, the signal $y_{(1,1)}$ segment into $y_{(2,1)}$ and $y_{(2,2)}$ by its B_1 and A_2. the signal $y_{(1,2)}$ segment into $y_{(2,3)}$ and $y_{(2,4)}$ by its B_1 and A_2. The boundaries of each signal segment are as follows:

$$y_{(2,1)} \in [0ns, 85ns], y_{(2,2)} \in [84ns, 153ns]$$

$$y_{(2,3)} \in [94ns, 220ns], y_{(2,4)} \in [137ns, 247ns]$$

For the dictionary update, four customized dictionaries $D_{(2,1)}$, $D_{(2,2)}$, $D_{(2,3)}$, and $D_{(2,4)}$ are generated for signal segment $y_{(2,1)}$, $y_{(2,2)}$, $y_{(2,3)}$ and $y_{(2,4)}$, respectively.

Similar to the initial sparse decomposition, the relaxation coefficient α is set to 1.5 empirically. Larger α leads to larger boundaries, ensuring the phase plane covered all the ultrasonic echoes inside the segment signal. However, this will lower the matching degree between the atoms and the true echoes. On the other hand, smaller α constrains the boundaries excessively, as a result, the true echoes lie outside the range $[\frac{sl_{(n,i)}}{\alpha}, \alpha su_{(n,i)}], [\frac{ul_{(n,i)}}{\alpha}, \alpha uu_{(n,i)}], [\frac{fl_{(n,i)}}{\alpha}, \alpha fu_{(n,i)}]$.

A value of approximately 1.5 for provides an appropriate balance according to experiments conducted. It rescales the parameter space sufficiently while avoiding excessive mismatched atoms.

The compressed boundaries of scale parameter for the dictionary $D_{(2,1)}$, $D_{(2,2)}$, $D_{(2,3)}$ and $D_{(2,4)}$ are obtained using equation (3).

$$s_{D_{(2,1)}} = [0.0347, 0.0781],\ s_{D_{(2,2)}} = [0.0364, 0.0819]$$

$$s_{D_{(2,3)}} = [0.0486, 0.1093],\ s_{D_{(2,4)}} = [0.0329, 0.0741]$$

Shorter signal segment leads to fewer sampling point for scale parameter and frequency. Thus, the discretization step of these two parameters in dictionary is further optimized by updating the variable a based on equation (6).

$$a_{new_{(2,1)}} = \sqrt[nsD_{2,1}]{su_{(2,1)}} = \sqrt[ns_{D_0}]{su_{(2,1)}} = 1.7238990$$

$$a_{new_{(2,2)}} = \sqrt[nsD_{2,2}]{su_{(2,2)}} = \sqrt[ns_{D_0}]{su_{(2,2)}} = 1.7500898$$

$$a_{new_{(2,3)}} = \sqrt[nsD_{2,3}]{su_{(2,3)}} = \sqrt[ns_{D_0}]{su_{(2,3)}} = 1.7975390$$

$$a_{new_{(2,4)}} = \sqrt[ns_{D_{(2,4)}}]{su_{(2,4)}} = \sqrt[ns_{D_0}]{su_{(2,4)}} = 1.7125922$$

The size of each dictionary can be calculated using equation (4).

$$L_{D_0} = 106496, L_{D_{(2,1)}} = 98833, L_{D_{(2,2)}} = 83160, L_{D_{(2,3)}} = 107328, L_{D_{(2,4)}} = 99197$$

The discretization step of the dictionary has been further refined without significantly increase their sizes. However, since there are still two atoms in each signal segment's sparse decomposition result, according to Case 2 of the termination criteria in Section 5, the algorithm proceeds to iteration 2.

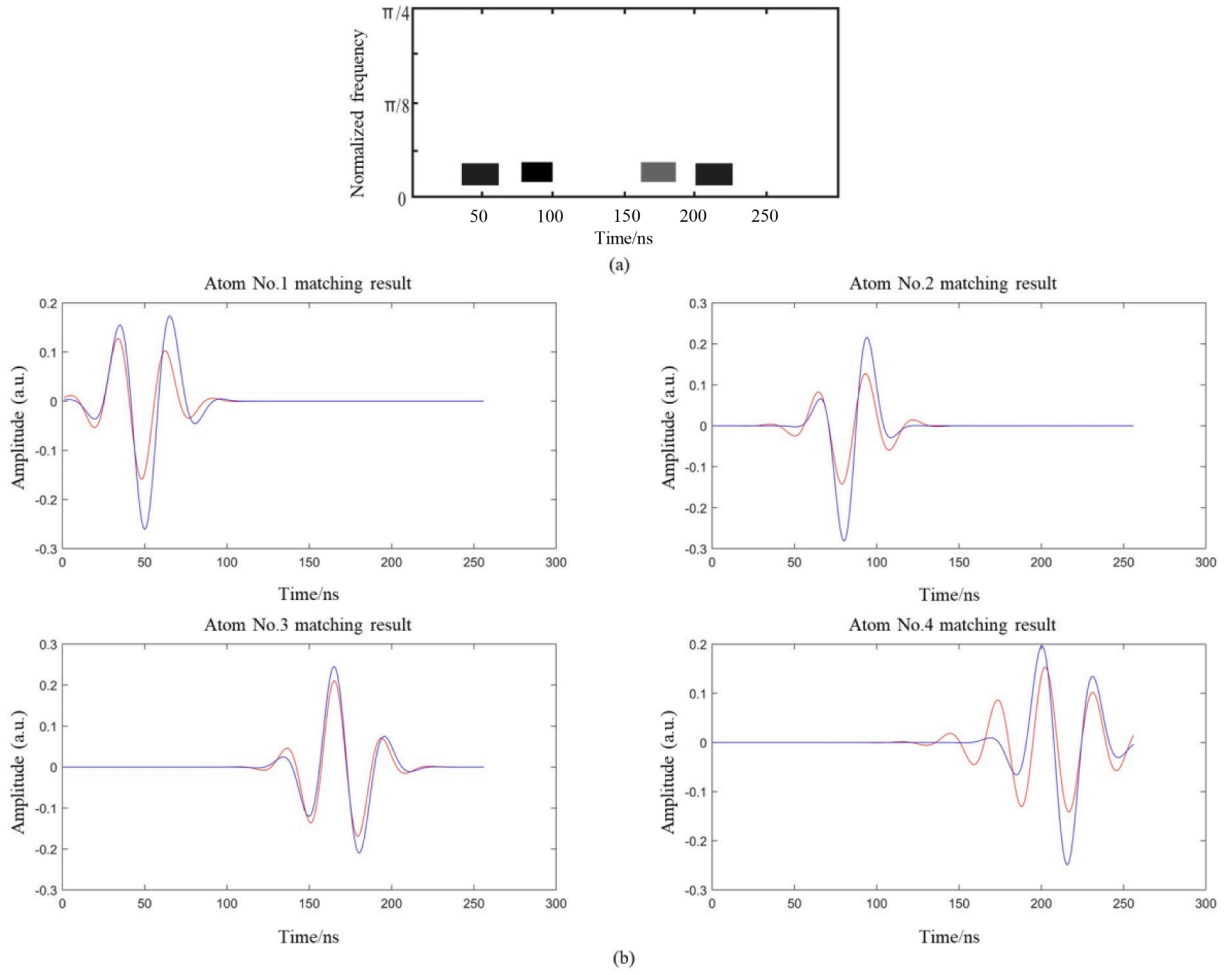

Fig. 7. The result of second iteration of the proposed algorithm (a) in phase plane. (b) Matching with the simulated echoes.

3) Iteration 2

In this iteration, signal segments $y_{(2,1)}$, $y_{(2,2)}$, $y_{(2,3)}$ and $y_{(2,4)}$ are decomposed using SMP with their corresponding dictionaries $D_{(2,1)}$, $D_{(2,2)}$, $D_{(2,3)}$, and $D_{(2,4)}$. The decomposed result and the reconstructed echoes are presented in Fig. 7. By setting the residual threshold ε equal to the initial sparse decomposition, only one atom is obtained for each signal segment decomposition. As the Case 1 termination criterion is met, the algorithm proceeds to termination.

In Fig. 7(b), the four subfigures are the matching comparisons between the four atoms obtained from the decomposition in Fig. 4(a) and the four echoes that compose the signal y. In these subfigures, the red curves represent the decomposed atoms, while the blue curves denote the initial echoes that make up signal y.

4) Termination

Since Case 1 of the termination criteria is met in iteration 2, it is necessary to determine which of the two possibilities the result belongs to. To do this, the dictionaries are further update to $D_{(3,1)}$, $D_{(3,2)}$, $D_{(3,3)}$, and $D_{(3,4)}$, and the signal segments $y_{(2,1)}$, $y_{(2,2)}$, $y_{(2,3)}$ and $y_{(2,4)}$ decomposed by SMP using the SMP algorithm with finer dictionaries $D_{(3,1)}$, $D_{(3,2)}$, $D_{(3,3)}$, and $D_{(3,4)}$, respectively. The residual threshold ε is set to 0.2. As only one atom obtained for each signal segment. Case 1.2 of the termination criteria is met. Consequently, the iteration terminates, and the sparse decomposition for signal y concludes.

6.2. Comparison of echo estimation between the traditional SMP and the proposed algorithm

The estimation accuracy was measured by three criteria: energy error, coefficient error, and amplitude error [24]. The energy error E_{error} is defined as:

$$E_{error} = \frac{\|\widetilde{y}_l - y_i\|}{\|y_i\|_2} \times 100\% \tag{9}$$

Where y_i is the original echo and $\widetilde{y}_l$ is the recovered echo. The coefficient error which measures the similarity of the decomposition solution is defined as:

$$C_{error} = \frac{\left|\left|\widetilde{c}_l\right| - |c_i|\right|}{|c_i|} \times 100\% \tag{10}$$

Where $\widetilde{c}_l$ is the estimated reflection coefficient and c_i is the reflection coefficient. The amplitude error which measures the performance of amplitude-polarity AMI is defined as:

$$A_{error} = \frac{|A_{rec} - A_{theo}|}{|A_{theo}|} \times 100\% \tag{11}$$

Where A represents the peak intensity value of recovered echo.

The algorithm under study, executed on a Lenovo laptop equipped with an Intel Core i5 processor and 8 GB of RAM, requires approximately 0.5 s to decompose a signal of length 256 utilizing a standard Gabor dictionary composed of 100,000 atoms. In terms of memory, the algorithm demands approximately 200 MB. Both the computation time and memory usage scale linearly with the signal length and the size of the dictionary. These metrics provide a current assessment of the algorithm's performance.

Table 3 displays the results for the simulated signal shown in Fig. 4. The results in Table 3 demonstrate that the traditional SMP algorithm is less accurate in processing highly overlapping ultrasonic echoes. Yet, the multiresolution sparse decomposition algorithm shows marked improvements in accuracy with subsequent iterations. Notably, the energy error for echo number 1 decreases dramatically from 32.59 % to 2.15 %, and both the coefficient error and amplitude error diminish from 38.02 % and 26.45 % to 2.22 % and 15.31 %, respectively. This equates to an enhancement in accuracy by approximately factors of 15, 16, and 1.7, respectively.

The simulation results are impressive; however, the algorithm's accuracy in real-world applications may be subject to variation due to material properties, environmental noise, and equipment variability, subsequently affecting its performance. In ultrasonic non-destructive evaluation (NDE), the Gabor function typically models real ultrasonic signals effectively, particularly during pulse-echo

Table 3
The echo estimation performance of proposed algorithm and traditional SMP algorithm.

		Echo 1	Echo 2	Echo 3	Echo 4
Traditional SMP	E_{error}(%)	32.59	65.02	47.74	56.95
Proposed algorithm		2.15	4.52	2.35	3.26
Traditional SMP	C_{error}(%)	38.02	42.49	21.28	28.33
Proposed algorithm		2.22	4.35	1.03	3.18
Traditional SMP	A_{error}(%)	26.45	50.83	20.68	28.49
Proposed algorithm		15.31	17.96	2.55	11.20

imaging using broadband transducers. However, when detecting Lamb waves, discrepancies from the Gabor model can emerge. When ultrasonic echoes are not precisely replicated by the Gabor function, the algorithm delineated in this study may retain its applicability, although its efficacy might be reduced, mirroring the outcomes when employing a conventional Gabor dictionary for ultrasonic signal decomposition. Therefore, experimental validation with genuine ultrasonic signals in multilayered electronic packaging is crucial to ascertain the algorithm's practical utility and dependability.

7. Experimental validation of multiresolution SSR algorithm

This section presents the experimental validation of the algorithm's decomposition capabilities on real signals acquired from multilayered electronic packaging. Two types of electronic packages, hidden-die and flip-chip, were selected as subjects for experimentation. Real A-scan signals from multiple points inside the packaging were collected using ultrasonic transducer with various frequencies. The characteristics of the transducer is shown in Table 4. These signals were then resolved using both the traditional SMP algorithm and the multiresolution sparse decomposition method proposed in this study. The comparative analysis aims to elucidate the efficiency and accuracy of the proposed method in handling real-world data scenarios.

Data acquisition was performed using a commercial scanning acoustic microscopy system, the Gen6™ C-scan, by Sonoscan. The excitation pulse, shape, and bandwidth are dependent on the transducer. The gain was established at 24.5, and the amplitude was influenced by this gain setting. The vertical resolution was configured to 8bit.

7.1. Experimental results for hidden-die packaging

7.1.1. Test samples and data collection

This section rigorously validates the algorithm's decomposition performance on hidden-dies, a form of embedded electronic packaging where the semiconductor die remains obscured beneath the package surface. To thoroughly assess the algorithm's ability to handle real, significantly overlapping A-scan signals, we employed the Virtual Resonance Mode (VRM) of the Sonoscan 6th Generation Acoustic Microscopy Imaging (AMI) system, paired with a 230 MHz high-frequency transducer, to conduct three-dimensional acoustic data collection on the samples. Subsequently, using our custom-developed toolbox, we extracted A-scan data from multiple locations within hidden-dies in the three-dimensional acoustic data. Finally, we conducted sparse decomposition on these signals employing both the traditional SMP algorithm and the multiresolution sparse decomposition algorithm introduced in this research. aiming to critically compare and ascertain the relative effectiveness of each algorithm in deconstructing these challenging signals.

Fig. 8 presents the C-scan top view image alongside the detailed structural configuration of the hidden-dies packaging. The embedded module has dimensions of 10 mm by 10 mm, while the chip itself measures 5 mm by 5 mm. The pitch between the chips is 100 μm, and each chip has a thickness of 50 μm. The die attach film (DAF) above the chips is 20 μm thick, followed by a 90 μm thick resin filling layer. The ultrasonic wave incidence point is 30 μm above the chip's upper surface. Beneath the DAF, a 12 μm thick copper plating layer is situated, under which lies the FR4 substrate that is 50 μm thick.

7.1.2. A-scan extraction using 3D acoustic microimaging toolbox

By performing sparse decomposition on A-scan signals composed of reflected echoes and using the atoms obtained from the decomposition to locate structures within the electronic packaging, the effectiveness of the proposed algorithm could be verified through comparison of these localization results with those derived from the traditional SMP algorithm as well as with computational outcomes based on the structural dimensions presented in Fig. 8. However, as the ultrasonic waves traverse through different locations of the electronic packaging encountering materials with varying properties, the characteristics of the reflected echoes exhibit significant differences. To further validate the effectiveness of the algorithm, this study extracts A-scan signals from different locations within electronic packaging. The collected three-dimensional acoustic data consist of A-scan signals from various measurement points of the sample. Consequently, the data are processed using a 3D toolbox previously developed by the team, enabling the extraction of A-scan signals from any location within the electronic packaging from the three-dimensional acoustic data. Fig. 9(a) demonstrates the user interface of the toolbox. After importing the 3D acoustic signal files, users can select any location on the C-scan image of the workpiece located at the lower left, whereupon the corresponding A-scan signal is displayed in the time-domain above. Furthermore, users have the option to select specific regions of the A-scan signal through a window, facilitating C-scan imaging at various depths of the workpiece. The toolbox is notably extensible, and the multiresolution sparse decomposition algorithm proposed in this study will be integrated into the software after experimental validation.

In this study, the A-scan signals from points A and B on the chip were used as examples to sparse decomposition using the traditional SMP algorithm with a standard Gabor dictionary and the algorithm proposed in this paper with a progressively refined Gabor dictionary. As can be deduced from the electronic packaging structure in Fig. 8, the signal at point A (coordinates (80,200)) did not pass through the chip, whereas the signal at point B (coordinates (160,200)) did. Fig. 9(b) and (c) display the A-scan signals

Table 4
Experimental parameters of ultrasonic transducer.

Frequency (MHz)	Focal length (inches)	Diameter (inches)	$F^{\#}$	Spot Size (mm)	Resolution (mm)	Depth of Focus (mm)
50	0.5	0.25	2	0.073	0.052	0.85
230	0.25	0.062	4	0.0321	0.0227	0.753

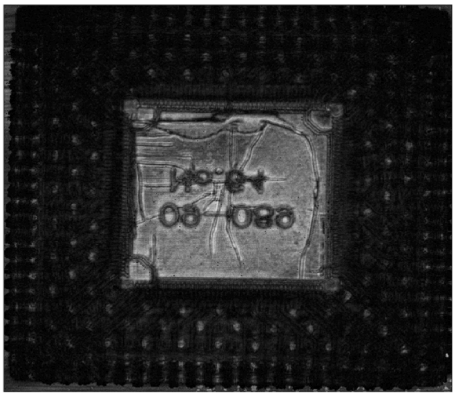

(a)

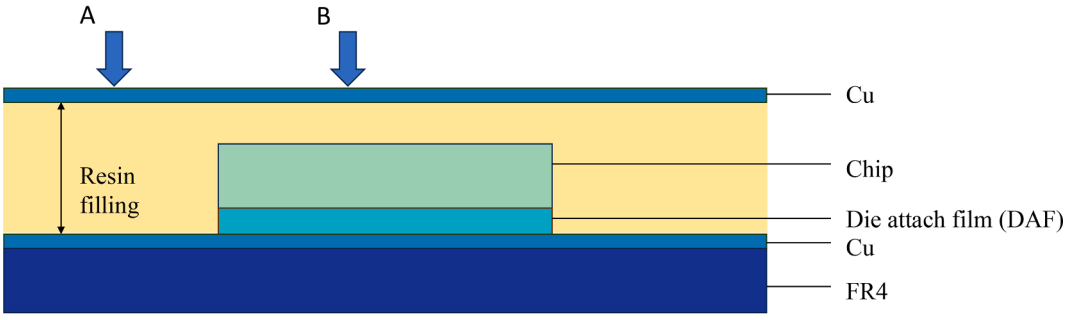

(b)

Fig. 8. (a) C-scan image of hidden-die packaging from the top view; (b) Schematic diagram of hidden-die structure.

extracted from the three-dimensional acoustic signals at points A and B using the Toolbox, with an ultrasound transducer frequency of 230 MHz. Fig. 9(d) and (e) present the sparse decomposition results in the phase plane for the signals in Fig. 9(b) and (c), utilizing the traditional SMP algorithm paired with the standard Gabor dictionary.

Since the ultrasonic signal at point A did not pass through the chip, the decomposition of the A-point ultrasonic signal should include three atoms according to the electronic packaging structure shown in Fig. 8, corresponding sequentially to the interface between the resin and the upper copper, the interface between the resin and lower copper, and the interface between lower copper and the board. However, the decomposition result shown in Fig. 9(d) only contains two atoms, indicating that the traditional SMP algorithm failed to effectively differentiate overlapping echoes.

Similarly, the ultrasonic signal at point B pass through the chip, the decomposition of the B-point ultrasonic signal should encompass five atoms, corresponding to the interface between upper copper and resin, upper surface of the chip, the interface between the chip and the DAF, the interface between the DAF and the lower copper, and the interface between the lower copper and the board. However, the decomposition result revealed in Fig. 9(e) only presents three atoms. The primary causes for these discrepancies include:

1. The multilayered structure of the chip at submicron scales results in a significant overlap of reflected echoes, and the standard Gabor dictionary used by the SMP algorithm does not have a sufficient number of parameter sampling points within the signal length, which affects the precise identification of echo locations.
2. The chip may experience warping deformation during usage due to mismatched thermal expansion of internal layers, moisture absorption, mechanical stress, etc., which significantly impacts the results of ultrasonic testing.

7.1.3. Decomposition results

The issue of overlapping echoes caused by the multilayer structure can be resolved through algorithmic optimization. The proposed algorithm was applied to the ultrasonic signals obtained from points A and B, with Figs. 10 and 11 illustrating the respective decomposition results.

As demonstrated in Fig. 10, the ultrasonic signal at point A was decomposed successfully after two iterations of the algorithm. Fig. 10(b) and (c) depict the atomic schematics after each iteration. Fig. 10(d) presents the reconstructed ultrasonic signal at point A using the atoms derived from Fig. 10(c). Fig. 10(e) shows the decomposition results in the phase plane. Similarly, as shown in Fig. 11,

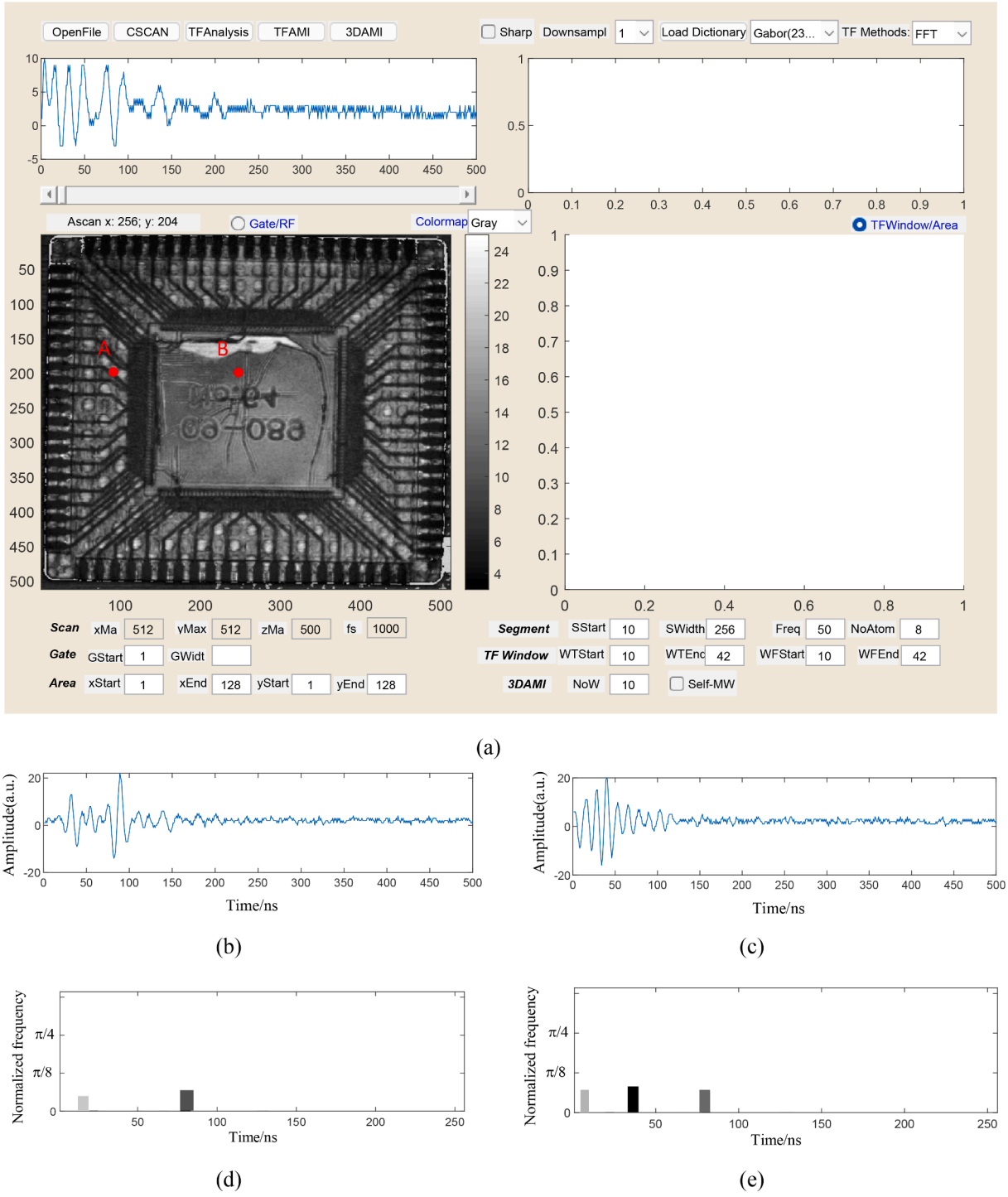

Fig. 9. (a) The GUI of the Toolbox for 3D Acoustic Imaging of Manufactured Electronic Circuits; (b) The a-scan signal of point A (80,200); (c) The a-scan signal of point B (160,200); (d) The decomposition results of the A scan signal from point A using SMP algorithm; (e) The decomposition results of the A scan signal from point B using SMP algorithm.

the algorithm terminated after three iterations when processing the ultrasonic signal at point B, with Fig. 11(b), (c), and (d) illustrating the atomic schematics after each iteration. Fig. 11(e) displays the reconstructed ultrasonic signal at point B using the atoms obtained from Fig. 11(d), and (f) presents the decomposition results within the phase plane.

A comparison of the decomposition results in Figs. 10 and 11 with those in Fig. 9 reveals that the overlapping ultrasonic echoes,

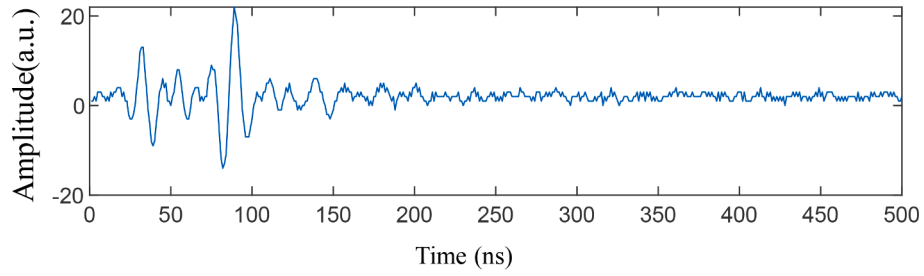

(a)

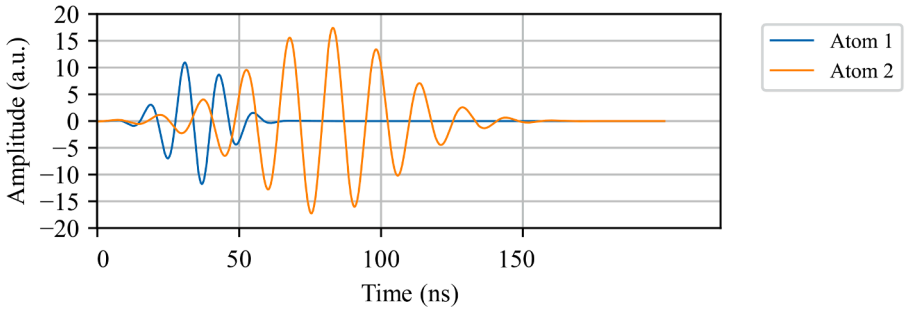

(b)

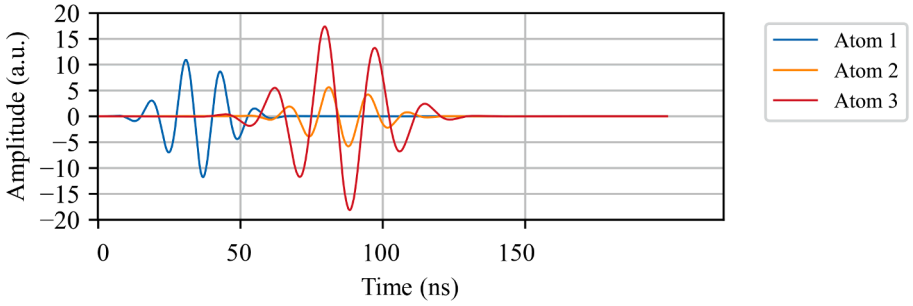

(c)

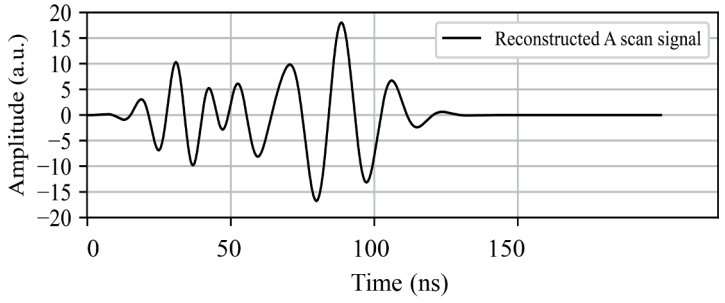

(d)

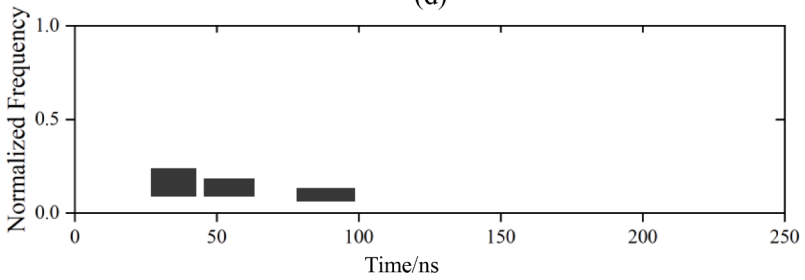

(e)

(caption on next page)

Fig. 10. Decomposition results for ultrasonic signal at point A using multiresolution sparse decomposition algorithm (a) A scan signal at point A; (b) decomposition result after first iteration; (c) decomposition result after second iteration; (d) reconstructed A scan signal; (e) final decomposition result in phase plane.

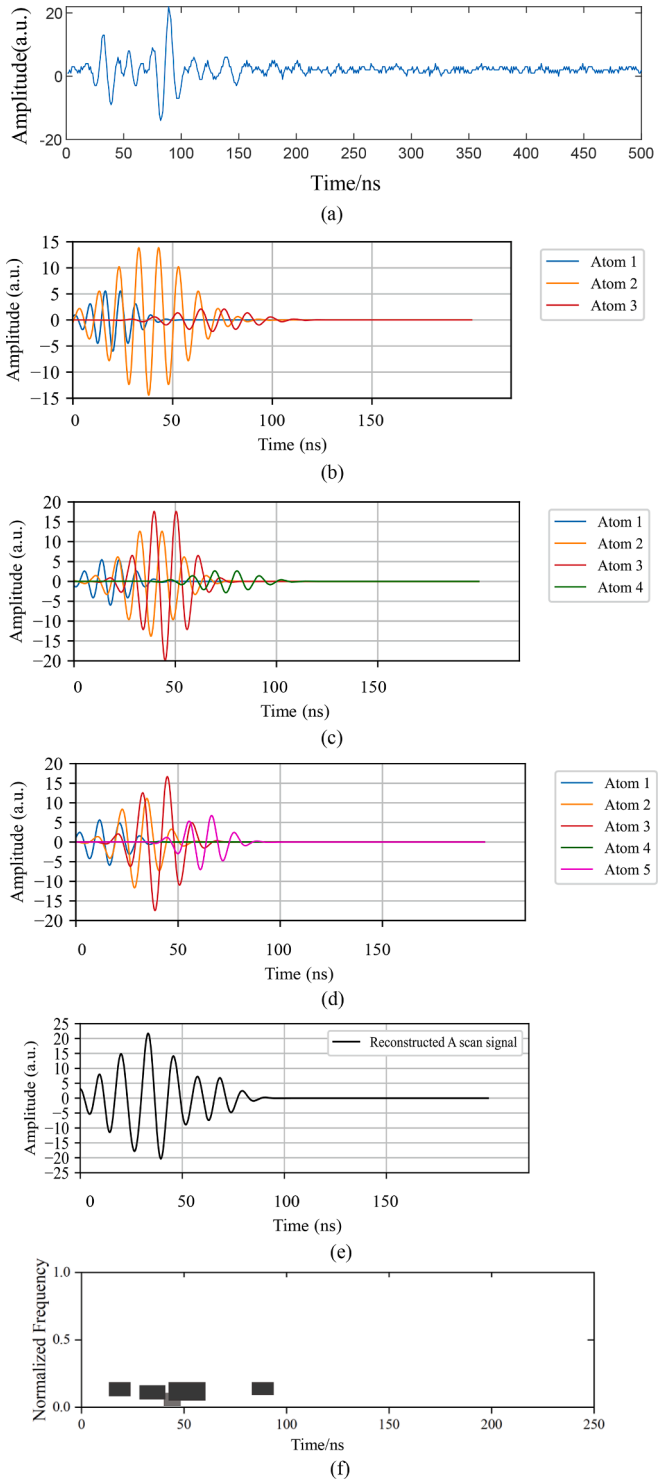

Fig. 11. Decomposition results for ultrasonic signal at point B using multiresolution sparse decomposition algorithm (a) A scan signal at point B; (b) decomposition result after first iteration; (c) decomposition result after second iteration; (d) decomposition result after third iteration; (e) reconstructed A scan signal; (f) final decomposition result in phase plane.

which could not be separated by the traditional SMP algorithm, are progressively distinguished under the proposed multiresolution sparse signal representation algorithm. This is attributed to the iterative process of the algorithm, where the signal is incrementally segmented into shorter sections, and sequentially coupled with a customized Gabor dictionary with gradually refined parameters. This ensures that the sparse decomposition of each signal segment achieves a higher resolution than the previous iteration.

An in-depth analysis and comparison of the decomposition results shown in Figs. 9, 10 and 11 indicates that the traditional SMP algorithm has significant limitations in distinguishing overlapping ultrasonic echoes. In contrast, the multiresolution sparse signal representation algorithm proposed in this study effectively addresses this issue. The warping deformation inherent in the encapsulated internal structure has led to discrepancies between the experimental findings and the theoretical predictions. Nevertheless, the proposed algorithm has adeptly segregated the overlapping echoes, a task at which the traditional SMP algorithm failed, thereby substantially enhancing the precision of echo localization. Within the framework of the s multiresolution sparse signal representation algorithm, the signal is initially divided into shorter segments, a process that facilitates the isolation of multiple echoes that are proximate in time domain. Subsequently, each signal segment undergoes sparse decomposition in conjunction with a progressively refined Gabor dictionary. This customized Gabor dictionary is parameterized based on the results of the previous iteration of the algorithm, ensuring that each iteration yields more precise decomposition results for the respective signal segments.

7.2. Experimental results for flip-chip packaging

Furthermore, it is essential to recognize that the complexity of echo overlap decomposition is influenced not only by the presence of multilayered structures but also significantly by the selection of ultrasonic transducer frequency. High-frequency transducers are characterized by their higher resolution yet suffer from limited penetration depth, while low-frequency transducers achieve greater penetration at the expense of resolution. To validate the algorithm's efficacy in decomposing A-scan signals obtained from identical chip locations with transducers of varying frequencies, a real automotive electronic circuit board (ceramic thick-film hybrid circuit) from a manufacturing line was used as the test sample to further validate the proposed algorithm. For the thick-film hybrid circuitry, multiple layers (tracks, conductors, dielectric layers, etc) were printed on one ceramic substrate. In this section, we focus on the flip-chip package on the ceramic board as illustrated in Fig. 12(b). The C-scan images for the solder bonds of the package are shown in Fig. 12(a). A scan at 32 points from different locations were investigated. Selected points are the representatives of two typical areas, point A: no solder joint area and point B: the center of solder balls area. At each point, A scan signals were captured using both 230 MHz transducer and 50 MHz transducer.

Fig. 13(a) and (b) display the A-scan signals obtained from regions without solder joints. Fig. 13(a) was acquired using a 230 MHz transducer, while Fig. 13(b) was captured with a 50 MHz transducer. As illustrated in Fig. 12(b), When ultrasonic waves traverse areas without solder joints, the reception of three main echoes is anticipated. The first echo corresponds to the interface between the chip and underfill, the second indicates the interface between the underfill and the thick film, and the third is from the reflection off the

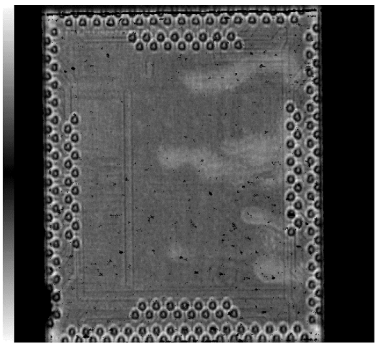

(a)

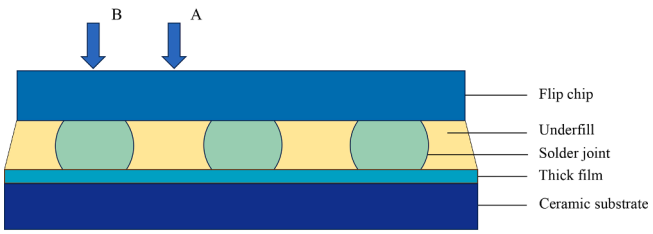

(b)

Fig. 12. (a) C-scan image of chip–solder bond interface produced from the detection of a flip-chip package soldered on a ceramic substrate; (b) Schematic diagram of flip-chip structure.

thick film's bottom surface. In Fig. 13(a), these three echoes are distinctly observed: the first echo occurs within the 50 to 100 ns range, the second is between 100 and 150 ns, and the third appears from 150 to 200 ns. In contrast, Fig. 13(b) shows that due to the ultrasonic probe's frequency being set at 50 MHz, the resolution is insufficient to differentiate these echoes.

The SMP algorithm, in conjunction with a Gabor dictionary, as well as the multiresolution sparse decomposition algorithm introduced in this study, was utilized to sparsely decompose the signals presented in Fig. 13(a) and (b), utilizing a progressively refined Gabor dictionary. Given that reflections are expected at three distinct interfaces, both methods extracted the first three atoms for the results display. Fig. 13(c) and (d) depict the phase plane distribution of atoms derived from the SMP algorithm, while Fig. 13(e) and (f) display the corresponding outcomes from the multi-resolution sparse decomposition algorithm. A comparative analysis indicates that the SMP algorithm exhibits significant variability in its decomposition capability for signals obtained from ultrasonic probes of different frequencies. By contrast, the multiresolution coefficient decomposition algorithm shows enhanced robustness with signals from probes at diverse frequencies. The gradual refinement of the dictionary parameters during the decomposition process permits the effective discrimination of highly overlapping echoes, thus improving echo localization accuracy. Therefore, this method provides a more precise imaging of the various interfaces within the encapsulation, markedly increasing the system's detection resolution.

Fig. 14 shows another case of example A scans from the center area of solder joint, where Fig. 14(a) depicts the ultrasonic signal obtained using a 230 MHz transducer, Fig. 14(b) demonstrates the signal acquired with a 50 MHz transducer. Further analysis of Fig. 12(b) reveals that the reflected signal within the solder joint area, akin to that in regions without solder joints, is composed of echoes from three interfaces: the interface between the chip and the solder joint, the interface between the solder joint and the upper surface of the thick film, and the interface between the thick film's bottom surfaces and the substrate. However, unlike the non-soldered areas, the signal in the solder joint region traverses through the solder ball material instead of underfill. Due to the

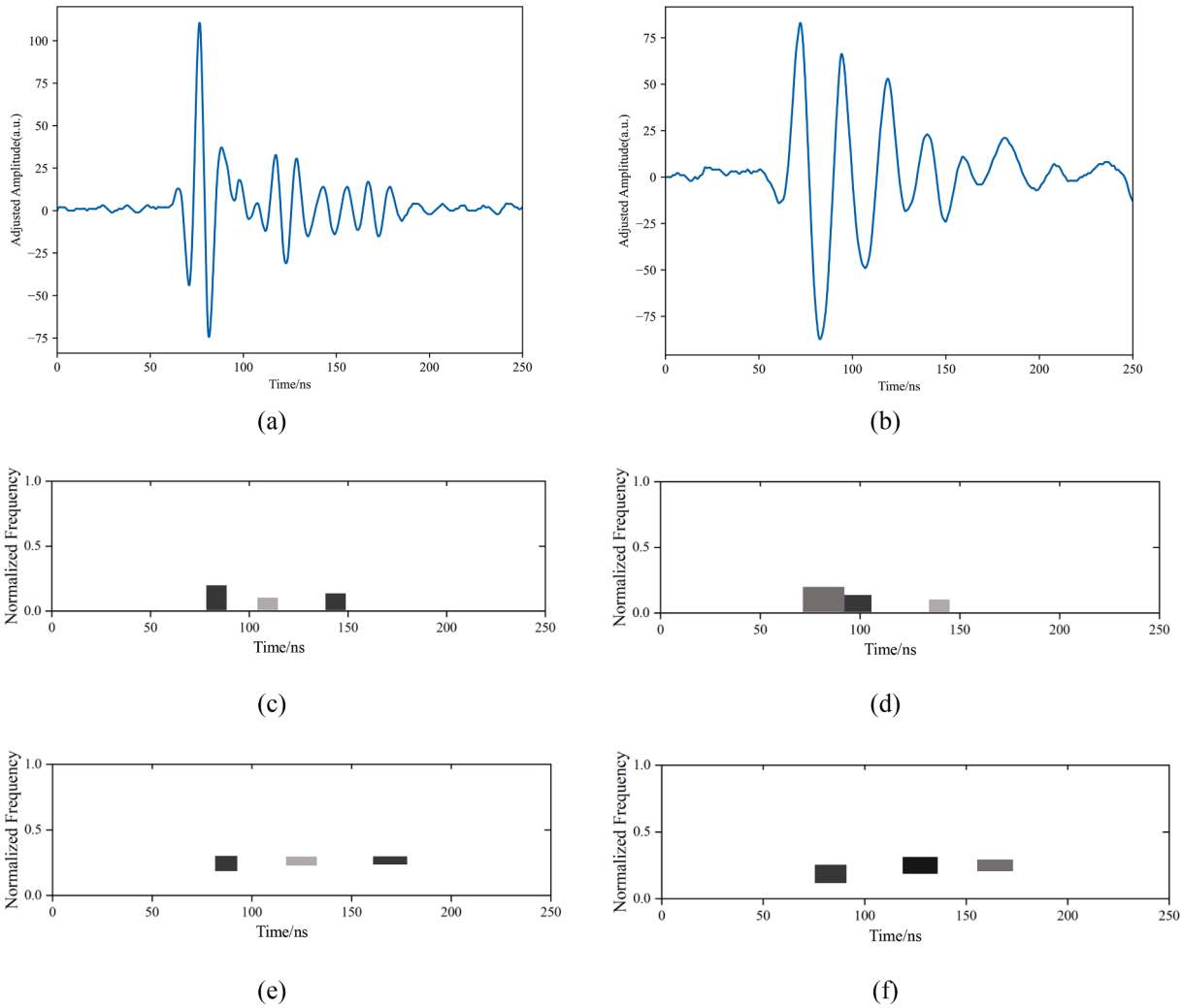

Fig. 13. A-scan signals obtained from non-solder joint area by (a) a 230 MHz transducer and (b) a 50 MHz transducer, decomposition results of each signal using the SMP algorithm are depicted in (c) and (d), respectively. The outcomes of the multiresolution algorithm's decomposition are presented in (e) and (f) correspondingly.

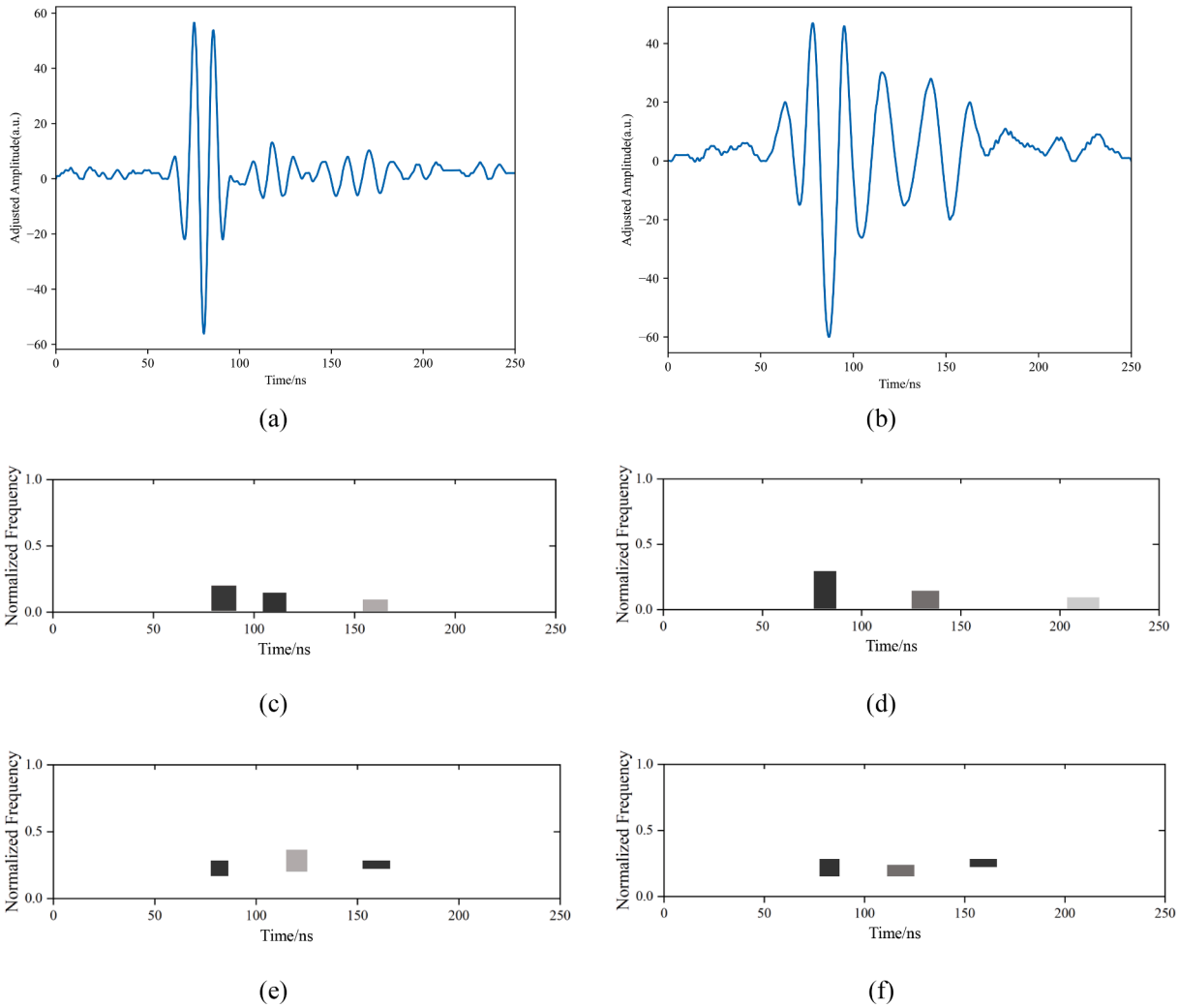

Fig. 14. A-scan signals pass through the centre of solder joint area captured by (a) a 230 MHz transducer and (b) a 50 MHz transducer, and the decomposition results of each signal using the SMP algorithm are depicted in (c) and (d), respectively. The outcomes of the multiresolution algorithm's decomposition are presented in (e) and (f) correspondingly.

relatively smaller acoustic impedance contrast between the solder ball material and the chip compared to that between the underfill and the chip, the echoes at these interfaces are weaker in the solder joint region.

Fig. 14(a) and (b) represent the A-scan ultrasonic signals captured by 230 MHz and 50 MHz transducers, respectively, as they pass through the central region of a solder joint. Fig. 14(c) and (d) illustrate the schematic of atoms in the phase plane obtained through sparse decomposition of the signals traversing the solder joint area using the SMP algorithm. Fig. 14(e) and (f) display the schematic of atoms in the phase plane resulting from the application of a multiresolution sparse decomposition algorithm. Consistent with the results in Fig. 13, the decomposition outcomes from the multiresolution sparse decomposition algorithm exhibit robust performance when dealing with ultrasonic signals captured at different frequencies. Moreover, when confronted with weak ultrasonic echoes as in Fig. 14(b), the SMP algorithm decomposition results shown in Fig. 14(d) present significant errors, isolating only two echoes in the main part of the signal (50 ns–150 ns) and misplacing the third echo around 220 ns. In contrast, the algorithm proposed in this study still achieves precise echo localization.

The experimental outcomes derived from the analysis of real-world signals have affirmed the efficacy of the multiresolution sparse signal representation algorithm introduced in this research. This algorithm exhibits substantial enhancements and shows promise for application in overcoming the resolution constraints and the overlapping echo dilemma prevalent in the traditional SMP algorithm. Such innovative advancements herald novel avenues for deployment in domains that necessitate exceptional precision, including advanced material evaluation and medical imaging.

8. Conclusions

This paper introduces a pioneering multiresolution analysis sparse signal representation algorithm, significantly enhancing current methodologies in ultrasonic echo separation and estimation. The algorithm's distinguishing feature is its iterative process of signal segmentation and dictionary refinement, enabling high-resolution decomposition without expanding the dictionary's dimensions. This novel method diverges substantially from conventional practices often constrained by resolution limitations and the management of extensive dictionary sizes.

Moreover, our innovative approach incorporates a tailored dictionary updating strategy for each segmented signal, which is predicated on the estimated echo parameters. This strategy considerably refines the alignment between dictionary atoms and echoes without necessitating expansive dictionary dimensions, offering a crucial advantage over traditional methods that rely on fixed, extensive dictionaries incapable of customization. Additionally, the simulation decomposition results proved our algorithm demonstrates potential in treating overlapping echoes, a prevalent challenge in ultrasonic Non-Destructive Evaluation (NDE). By utilizing refined dictionaries to decompose at more detailed scales, our algorithm improves both echo separation and estimation accuracy by iteration, even for echoes unresolved at coarser scales by standard techniques. To evaluating the performance of the proposed algorithm, energy error, coefficient error, and amplitude error of each echo were used as metrics, and the decomposition results were compared with those of the traditional SMP algorithm. The results indicate a significant reduction in error across all three metrics for the proposed algorithm: the average energy error decreased from 50.575 % to 3.07 %, the average coefficient error from 32.53 % to 2.695 %, and the average amplitude error from 31.6125 % to 11.755 %. This advancement not only elevates the efficacy of ultrasonic NDE but also lays a foundation for future research in sparse signal representation and analysis.

Experimental evaluations using real-world signals from microelectronic packages have validated the effectiveness of the proposed algorithm. The results indicate that the algorithm is capable of both overcoming the resolution constraints and the issue of overlapping echoes, which are prevalent in traditional methods. Moreover, the algorithm exhibits excellent performance on accurate echo estimation when processing A-scan signals acquired by ultrasonic transducer across a range of frequencies. This potent capability is especially relevant for applications that demand high precision.

CRediT authorship contribution statement

Haotian Wang: Writing – review & editing, Writing – original draft, Visualization, Validation, Software, Methodology, Formal analysis, Data curation. **Guangming Zhang:** Writing – review & editing, Supervision, Project administration, Methodology, Funding acquisition, Conceptualization. **Hongwei Ma:** Supervision, Project administration, Investigation, Funding acquisition. **Xuhui Zhang:** Writing – review & editing, Supervision. **Yuan Chen:** Writing – review & editing, Supervision. **David M. Harvey:** Writing – review & editing, Supervision, Project administration.

Declaration of competing interest

The authors declare that they have no known competing financial interests or personal relationships that could have appeared to influence the work reported in this paper.

Data availability

The authors do not have permission to share data.

Acknowledgements

This work was supported in part by the COP26 Trilateral Research Initiative by the British Council. This work was supported in part by the EU H2020-Marie Sklodowska-Curie research and innovation staff exchange 2019 grant (No. 871163), and the National Natural Science Foundation of China (Nos. 61674121, & 51705418). Many thanks to Mr. Andy Lloyd and Mr. Jim Papworth formally from Delphi Technologies, Kirkby, UK for their assistance in performing the ATC testing.

References

[1] H. Zhang, et al., The auto-correlation of ultrasonic lamb wave phased array data for damage detection, Metals 9 (6) (2019) 666.
[2] N. Mahal, K.Y. Houman, A.K. Nandi, Improved defect detection using adaptive leaky NLMS filter in guided-wave testing of pipelines, Appl. Sci. 9 (2) (2019) 294.
[3] G.-M. Zhang, D.M. Harvey, Contemporary ultrasonic signal processing approaches for nondestructive evaluation of multilayered structures, Nondestructive Test. Eval. 27 (1) (2012) 1–27.
[4] X. Yang, et al., Comparative study of ultrasonic techniques for reconstructing the multilayer structure of composites, NDT & E Int. 121 (2021) 102460.
[5] J. Choi, J.-W. Hong, Characterization of wavelet coefficients for ultrasonic signals, J. Appl. Phys. 107 (2010) 11.
[6] R. Fuentes, et al., A probabilistic compressive sensing framework with applications to ultrasound signal processing, Mech. Syst. Signal Process. 117 (2019) 383–402.
[7] J.M. Druce, J.D. Haupt, S. Gonella, Anomaly-sensitive dictionary learning for structural diagnostics from ultrasonic wavefields, IEEE Trans. Ultrason. Ferroelectr. Frequency Control 62 (7) (2015) 1384–1396.
[8] G.-M. Zhang, D.M. Harvey, D.R. Braden, An improved acoustic microimaging technique with learning overcomplete representation, J. Acoust. Soc. Am. 118 (6) (2005) 3706–3720.
[9] Y. Li, K. Yao, X. Li, An ultrasonic signal reconstruction algorithm of multilayer composites in non-destructive testing, Appl. Acoust. 186 (2022) 108461.

[10] K. Baishya, et al. "Toolbox for 3D acoustic imaging of manufactured electronic circuits." 2016 6th Electronic System-Integration Technology Conference (ESTC). IEEE, 2016.
[11] Tan, Shihong, et al. "Denoising method of high-frequency ultrasonic detection signals of flip chip based on orthogonal matching pursuit optimized by artificial bee colony." 12th International Conference on Quality, Reliability, Risk, Maintenance, and Safety Engineering (QR2MSE 2022). Vol. 2022. IET, 2022.
[12] X. Hong, J. Zhou, Y. He, Damage detection of anchored region on the messenger cable based on matching pursuit algorithm, Mech. Syst. Signal Process. 130 (2019) 221–247.
[13] S. Hamidi, S. ShahbazPanahi, Sparse signal recovery-based imaging in the presence of mode conversion with application to non-destructive testing, IEEE Trans. Signal Process. 64 (5) (2015) 1352–1364.
[14] L. Su, et al., An improved orthogonal matching pursuit method for denoising high-frequency ultrasonic detection signals of flip chips, Mech. Syst. Signal Process. 188 (2023) 110030.
[15] G.-M. Zhang, C.-Z. Zhang, D.M. Harvey, Sparse signal representation and its applications in ultrasonic NDE, Ultrasonics 52 (3) (2012) 351–363.
[16] X. Li, et al., Research on sparse decomposition processing of ultrasonic signals of heat exchanger fouling, IEEE Sens. J. (2023).
[17] E. Mor, M. Aladjem, A. Azoulay, A sparse approximation method for ultrasonic monitoring the degradation of adhesive joints, NDT & E Int. 98 (2018) 17–26.
[18] Kirchhof, Jan, et al. "Sparse signal recovery for ultrasonic detection and reconstruction of shadowed flaws." 2017 IEEE International Conference on Acoustics, Speech and Signal Processing (ICASSP). IEEE, 2017.
[19] J.A. Tropp, Greed is good: Algorithmic results for sparse approximation, IEEE Trans. Inf. Theory 50 (10) (2004) 2231–2242.
[20] E. Mor, A. Azoulay, M. Aladjem, A matching pursuit method for approximating overlapping ultrasonic echoes, IEEE Trans. Ultrason. Ferroelectr. Frequency Control 57 (9) (2010) 1996–2004.
[21] S.G. Mallat, Z. Zhang, Matching pursuits with time-frequency dictionaries, IEEE Trans. Signal Process. 41 (12) (1993) 3397–3415.
[22] Y. Lu, J.E. Michaels, Numerical implementation of matching pursuit for the analysis of complex ultrasonic signals, IEEE Trans. Ultrason Ferroelectr. Frequency Control 55 (1) (2008) 173–182.
[23] S.S. Chen, D.L. Donoho, M.A. Saunders, Atomic decomposition by basis pursuit, SIAM Rev. 43 (1) (2001) 129–159.
[24] G.-M. Zhang, D.M. Harvey, D.R. Braden, Advanced acoustic microimaging using sparse signal representation for the evaluation of microelectronic packages, IEEE Trans. Adv. Packaging 29 (2) (2006) 271–283.